Geothermal Energy

RESEARCH Open Access

Finite element simulation of permeable fault influence on a medium deep borehole thermal energy storage system

Lukas Seib[1*], Bastian Welsch[2], Claire Bossennec[1], Matthis Frey[1] and Ingo Sass[1,3,4]

*Correspondence:
seib@geo.tu-darmstadt.de

[1] Institute of Applied Geosciences, Geothermal Science and Technology, Technical University of Darmstadt, Schnittspahnstraße 9, 64287 Darmstadt, Germany
[2] Bochum University of Applied Sciences, Am Hochschulcampus 1, 44801 Bochum, Germany
[3] Darmstadt Graduate School of Excellence Energy Science and Engineering, Technical University of Darmstadt, Otto-Berndt-Straße 3, 64287 Darmstadt, Germany
[4] GFZ German Research Centre for Geosciences, Section 4.8: Geoenergy, 14473 Telegrafenberg, Potsdam, Germany

Abstract

Solutions for seasonal energy storage systems are essential for the reliable use of fluctuating renewable energy sources. As part of the research project SKEWS, a medium deep borehole thermal energy storage system with a depth of 750 m is under construction at Campus Lichtwiese in Darmstadt, Germany, to demonstrate this innovative technology. Prior to the design of SKEWS, the geological context in the surroundings of the project location was investigated using archive drilling data and groundwater measurements. The geologic survey suggests the assumption that the uppermost part of the intended storage domain is crosscut by a normal fault, which displaces the Permian rocks east of Darmstadt against granodioritic rocks of the Odenwald crystalline complex. A 3D finite-element numerical model was implemented to estimate the effect of the potentially higher hydraulic conductivity of the fault zone on the planned storage system. For this purpose, a storage operation over a time span of 30 years was simulated for different parametrizations of the fault zone. The simulations reveal a limited but visible heat removal from the storage region with increasing groundwater flow in the fault zone. However, the section of the borehole thermal energy storage system affected by the fault is minor compared to the total depth of the system. This only constitutes a minor impairment of the storage efficiency of approximately 3%. In total, the amount of heat extracted varies between 320.2 GWh and 326.2 GWh for the different models. These findings can be helpful for the planning and assessment of future medium deep borehole thermal energy storage systems in fractured and faulted crystalline settings by providing data about the potential impact of faults or large fractures crosscutting the storage system.

Keywords: Medium deep-BTES, Fault permeability, Basement rock, FE-model

Introduction

In 2018, the final energy consumption in German households was primarily dominated by heat consumption, with 68.2% associated with space heating and 1% domestic hot water production (BMWI 2020). That is why the efficient design of the heat supply using new technologies is of great importance to reduce fossil fuel consumption and thus reduce greenhouse gas emissions. Much unused potential for heat supply lies in solar thermal energy and the cogeneration of heat and power (CHP). One problem that lowers

the potential of these technologies goes back to the significant seasonal variation in heating demand. Since CHPs are mainly operated to follow the heat demand, the power plants are throttled during the summer due to the reduced heat demand.

Consequently, the electricity output is reduced as well. Solar thermal energy suffers from similar problems as not all potential heat can be used due to the low heat demand during summer. In winter, on the other hand, the heat demand is so high that it cannot be covered entirely by solar thermal energy and CHP without providing an uneconomically large excess capacity. For this reason, fossil heat sources, such as boilers, are still frequently used to cover peak loads (Schaumann and Schmitz 2010). One solution to this problem is the seasonal storage of the summer excess heat to make it available for heating during winter.

An innovative technology for seasonal heat storage is a borehole thermal energy storage (BTES) system, in which the fed-in heat is stored in the natural subsurface. BTES consist of multiple boreholes that are usually not much deeper than 100 m (Dincer and Rosen 2007). The boreholes are completed with coaxial borehole heat exchangers, a system of closed pipes that is backfilled with cement-based grout. By circulating a heat carrier fluid through the pipes, heat can be conductively exchanged with the subsurface (Reuss 2015). Such design allows the utilization of a defined subsurface heat storage volume. So far, these systems have relied on comparatively shallow geothermal heat exchangers. A detailed description of existing BTES systems is available in the literature (Gehlin 2016; Welsch 2019).

Medium deep-BTES (MD-BTES) systems are a promising, new approach for the effective storage of excess heat (Bär et al. 2015). Numerical studies (Welsch et al. 2016) found that MD-BTES can be used to store multiple GWh of thermal energy per year with a recovery rate of up to 83%. Additionally, an environmental and economic assessment reveals major improvements for CHP-based district heating systems with integrated MD-BTES, reaching a decrease in greenhouse gas emissions of up to 4% (Welsch et al. 2018). As illustrated in Figure 1, shallow systems often access the topmost aquifer. Consequently, a thermal impact on groundwater cannot be

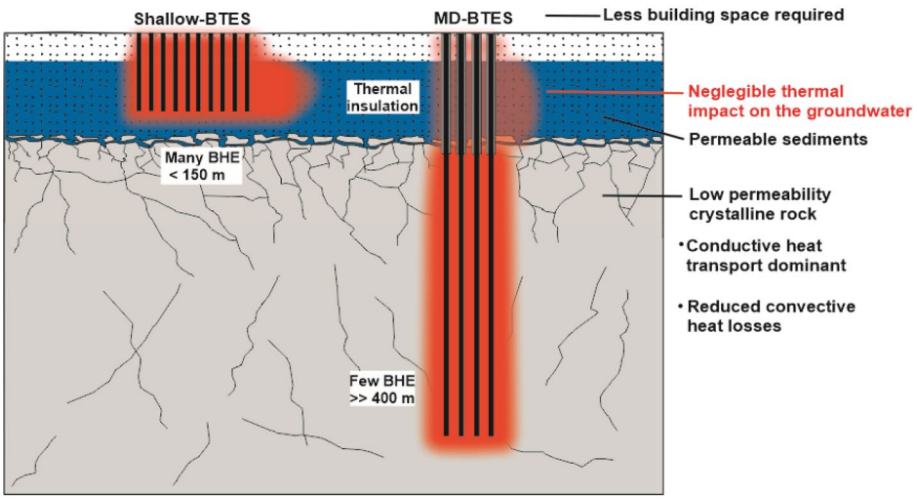

Fig. 1 Characteristics of a medium deep borehole thermal energy storage system (modified after Sass et al. 2016)

excluded (Griebler et al. 2015). The demand to store renewable heat in urban areas will increase dramatically, so conflict of use of the resources has to be mitigated. With MD-BTES, the heat is stored in a deeper part of the subsurface, which allows for the thermal insulation of BTES sections from the groundwater, thus reducing the temperature increase in the aquifer.

Furthermore, the low permeability of particular deeper formations reduces the convective water flow-related heat loss. Additionally, MD-BTES requires less surface space than shallow BTES specifically—a feature particularly helpful in urban areas (Welsch 2019). Similar concepts also exist for medium deep ATES systems, that can be utilized to negate the impact on shallow aquifers (Kranz and Frick 2013; Blöcher et al. 2019). MD-BTES are different from deep borehole heat exchangers (DBHE) (Kohl et al. 2002) because of their intended purpose and array layout. DBHE may have a depth between 1 km and 3 km with the main purpose of heat extraction or extraction with a regeneration phase during the summer (Liu et al. 2020; Luo et al. 2021; Chen et al. 2019). In contrast, MD-BTES are designed for an optimal heat storage performance. The wellbore spacing of the BHE is chosen to be small enough to allow for interaction between the BHE, while maximizing storage volume at the same time. The depth of MD-BTES is limited, as a longer dwelling time of the heat carrier fluid in the storage increases heat loss (Welsch et al. 2016).

However, the feasibility and efficiency of MD-BTES have been proven by numerical simulations so far (Schulte et al. 2016a; Welsch et al. 2016). Therefore, a pilot MD-BTES system is under construction at the Lichtwiese campus of the Technical University of Darmstadt, Germany, as part of the research project SKEWS (Seasonal crystalline Medium Deep Borehole Energy Storage System). For this pilot system, the construction of four medium deep borehole heat exchangers with a depth of 750 m each is targeted (Fig. 1). In case of success, the storage system is expected to be enlarged to 19 BHE in a first and 37 BHE in a second stage of expansion.

Hydrogeological and geological investigations were carried out at the project site to provide a simplified geological model of the borehole thermal energy storage system. The software FEFLOW (Diersch 2014) was used to simulate the effects of the planned storage site on the subsurface and test the planned loading and unloading scheme for applicability. Geologic pre-investigation at the site suggested the presence of a fault zone in the vicinity of the drill positions. Since fault zones can act as fluid pathways, they can increase heat transport from the storage, decreasing the efficiency of the operation. This study deals with quantifying geological fault zones effect on the energetic efficiency of a conductive underground heat storage system.

Since previous studies about the behavior and characteristics of MD-BTES systems considered simplified, homogeneous models, the real severity of the effects caused by geological heterogeneities on the performance of MD-BTES systems is not quantified. Since no specific characteristics of the fault zone are known so far, a simplified representation of a fault was implemented into the model, to get valuable insights into the impairment of the storage performance by a permeable zone. The effect of the variation of the main characteristics of the fault zone (i.e., its hydraulic conductivity and thickness) was tested in a parameter study to capture the range of potential impacts.

Test site—geological context

The project site is located in the southeast of Darmstadt, Germany. The geologic context is governed by the main eastern fault of the Upper Rhine Graben, which divides the city geologically (Fig. 2). The eastern part of the reported site herein is characterized by fracture-controlled igneous, volcanic and sedimentary rocks of the Odenwald and Sprendlinger Horst, wherein the BTES site is installed (Klemm 1911; Greifenhagen 2000).

The Odenwald crystalline complex is the largest outcropping massif of the Mid-German Crystalline High and belongs to the northern margin of the variscan orogen. The Frankenstein complex's northernmost unit consists of pyroxene, hornblende, and olivine gabbros and diorites on the southern margin. Its northern part underlying the city of Darmstadt and the so-called Sprendlinger Horst is built of paragneiss, granodiorite and granite (Dörr and Stein 2019; Stein 2001; Mezger et al. 2013). During the late Carboniferous and Permian, crustal extension led to the establishment of several intramountainous basins, later filled with sediments in arid climates in the area of the Sprendlinger Horst (Greifenhagen 2000; Aretz et al. 2016). The resulting conglomerates, claystones and sandstones of the sedimentary cover of the Sprendlinger Horst are locally interbedded with basalts as a product of permo-carboniferous volcanism (Al-Malabeh and Kempe 2009). During the Cenozoic the regional geology was affected by the opening of

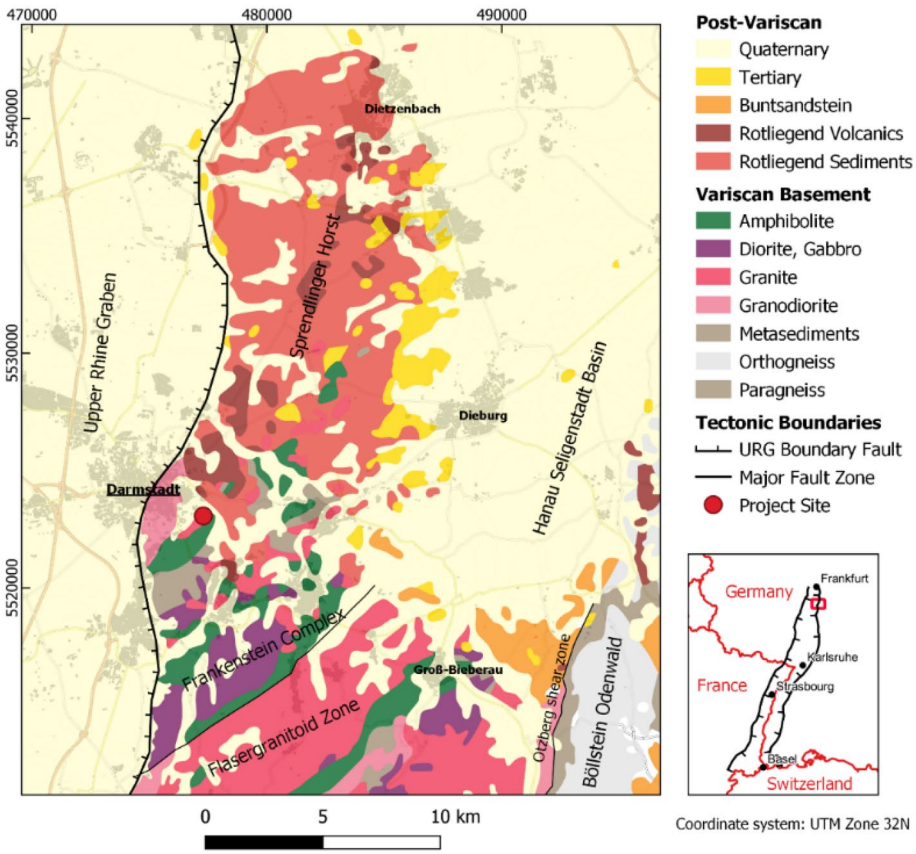

Fig. 2 Geologic overview of the Sprendlinger Horst and northern Odenwald (modified after GÜK300 Hessen, HLNUG (2007))

the Upper Rhine Graben (Schumacher 2002; Derer et al. 2005) and associated volcanic activity (Mezger et al. 2013).

The western part of Lichtwiese Campus consists of granodiorite of the Frankenstein Complex under a thin 2–6 m cover of quaternary sediments (Fig. 3). The upper basement is characterized by a weathering zone with a variable depth of up to 40 m (Greifenhagen 2000). Locally, this zone might be even larger, which became evident by the drillings. It is composed by the weathering products of the granodiorite, with monocrystalline and lithoclast grains whose granulometry ranges from sand to medium gravel size. In the North, East and South of Lichtwiese Campus, coarse to fine-grained sands originating from weathered Permian redbeds unconformably overlay the Variscan basement units. Previous research suggests the interpretation of the North–South oriented boundary separating the granodiorites from the Permian as a fault zone (Fahlbusch 1975, 1980; Klemm 1938; Kempe et al. 2001; Lang et al. 2011; Backhaus 1965). This fault or a similar one was hit by the first of four BHE drillings recently.

Material and methods

The wider SKEWS project area is penetrated by several geotechnical drillings and multiple groundwater monitoring wells. This data was extracted and evaluated from the Hessian drilling database (HLNUG 2020). Hence, a first-order geologic and hydrogeologic model concept was developed and implemented into FEFLOW.

Geologic and hydrogeologic exploration

A total of 325 drilling datasets from the archive dating from 1950 to 2020 were provided by the Hessian agency for Nature Conservation, Environment and Geology (HLNUG) and evaluated to gain additional information about the local distribution of the different lithologies (Fig. 3a)

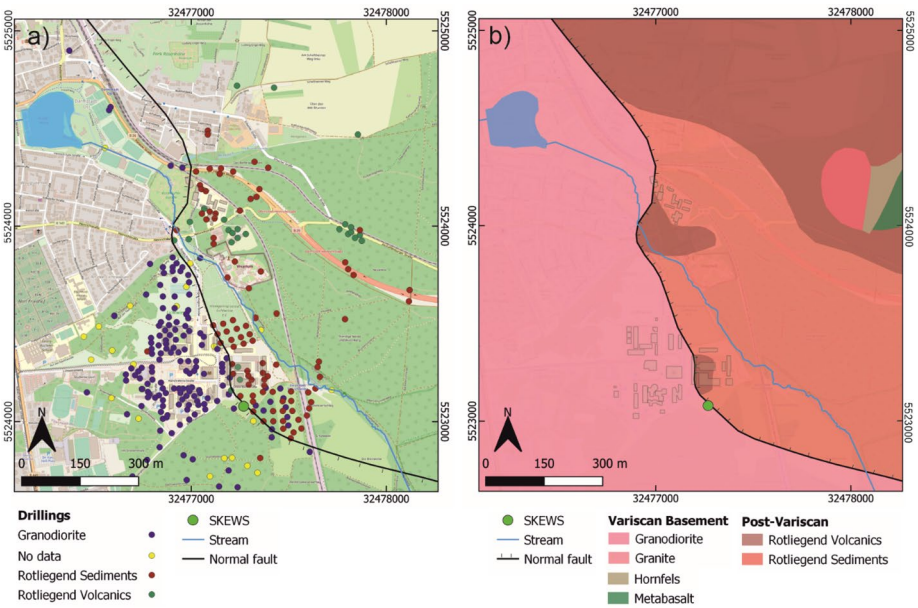

Fig. 3 **a** Drilling positions colored according to the explored lithology. **b** Geological map of the Lichtwiese campus (modified after Klemm 1911 and Fahlbusch 1980)

The evaluation of the drilling database allowed more precise localization of the suspected fault zone. After surveying the litho-logs, the fault zone was assumed in the eastern part of Lichtwiese Campus close to the planned MD-BTES. The information gained from the drilling data was imported into the suite ESRI ArcGIS. An interpolator was then used to create a raster file representing each geologic unit's depth map. Since only shallow drillings were available for the sedimentary Rotliegend in the east, a thickness of 40 m on top of the crystalline basement was assumed based on a minimal thickness of Rotliegend Sediments observed in drillings close to the suspected fault 350 m north of Lichtwiese campus.

To parametrize the groundwater model, data of 42 monitoring wells were used to generate transient contours with a monthly resolution (Fig. 4). The data were evaluated from 2000 to 2020. A monthly average of the hydraulic head was calculated for each monitoring well to integrate the dynamics of the hydraulic head.

The resulting single aquifer piezometric map shows a south–north direction of groundwater flow, which deviates to the west at the North of Campus Lichtwiese towards the URG (Fig. 4). The depth of the phreatic surface displays an average of

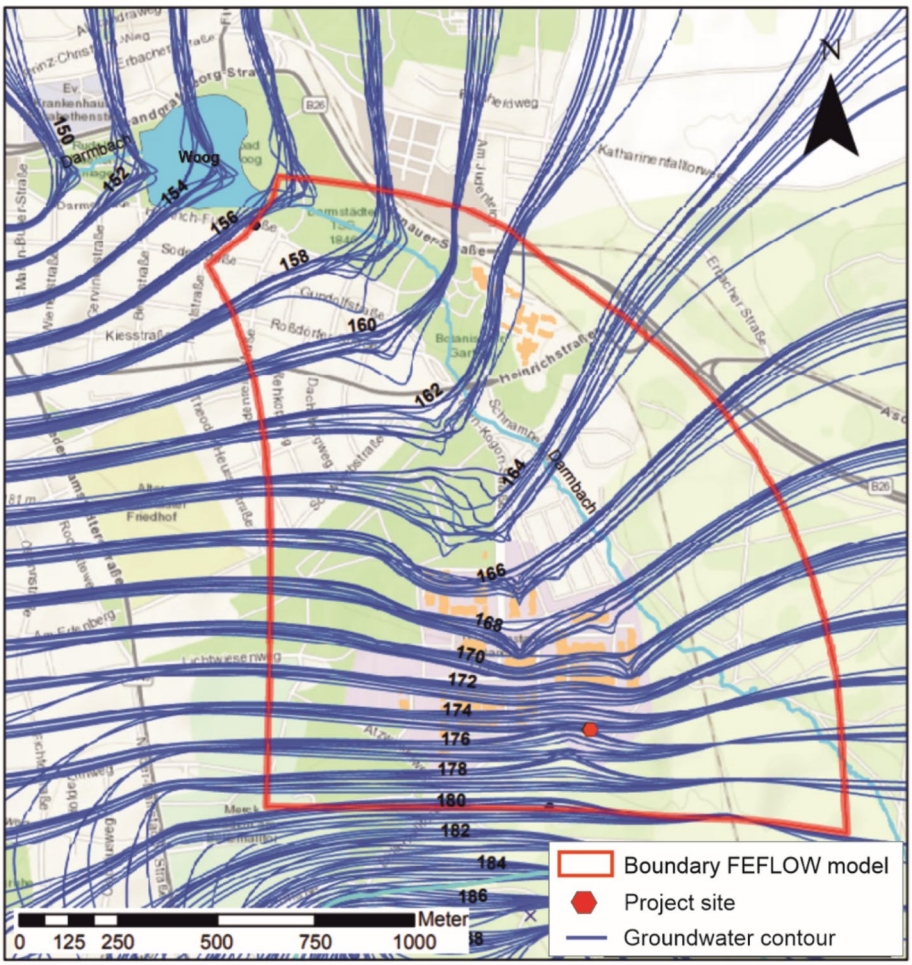

Fig. 4 Average groundwater contour lines for each month for the period 2000–2020. In red the FEFLOW model boundary, derived from the groundwater flow direction

approx. 5 m below surface. The model boundary for the FEFLOW model was based on the groundwater contours and the flow lines of the groundwater table. The goal of the chosen model boundary is to minimize the influences of the model boundary conditions on the BTES by providing sufficient separation between the boundary conditions and the MD-BTES. Additionally, the model was extended to the North to investigate the potential thermal influence on nearby water bodies like the Woog pond (Fig. 4).

Finite element model

The construction of the SKEWS system is planned with up to 4750-m-deep pilot borehole heat exchangers. This study was finished in the period of the drilling operation. Therefore, a simplification of the complicated geological conditions that were entcountered had to be made. A preliminary study on the storage test operation performed within the SKEWS project revealed a negligible thermal impact on the aquifer. However, a step-wise enlargement to 37 BHE in total is envisaged after the successful finalization of the SKEWS project following the pre-calculated storage models. Consequently, the investigations within this study consider the regular seasonal operation of a storage system that comprised all 37 BHE. The BHE array has a hexagonal shape with a BHE spacing of 5 m (Fig. 5). Due to their enhanced robustness in higher depth, coaxial pipe systems are used in SKEWS. In theory, coaxial BHE is advantageous because the flow direction can be reversed to reduce heat loss during loading and unloading cycles (Welsch et al. 2016), which could not be implemented due to the limitations of the FEFLOW-internal BHE solution. Furthermore, a thermal insulation of the upper part of the BHE, for example with the tool BASIMO (Schulte et al. 2016b, c), is not implemented in the model for reasons of simplification. The parametrization of each BHE is displayed in Table 1.

The FEFLOW model covers an area of 2 km^2. Its depth was set to 1000 m to prevent an influence of the lower boundary conditions on the BHE. A structured mesh of prismatic finite elements was used (Fig. 6), consisting of 87 mesh layers. Moreover, the mesh was refined around the BHE positions and closer to the fault zone to obtain better calculation results, where high-temperature variations or steps in the material properties due to the fault displacement are likely to occur (Fig. 6). The BHE are implemented as a particular type of boundary condition, at which it is possible to add or extract a defined amount of heat into the model (Diersch 2014). A dual continuum approach was applied for BHE

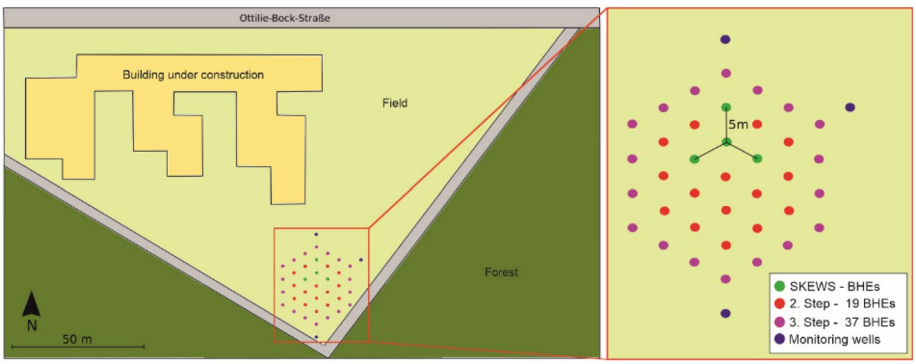

Fig. 5 Location and layout of the planned MD-BTES with the three building stages and additional groundwater monitoring wells

Table 1 Parameters of the coaxial borehole heat exchangers

BHE geometry	Coaxial
Borehole diameter	0.203 m
Inlet pipe diameter	0.1143 m
Outlet pipe diameter	0.1683 m
Refrigerant thermal conductivity	0.48 W m^{-1} 1 K^{-1}
Refrigerant volumetric heat capacity	4 MJ m^{-3} K^{-1}
Computational method	Quasi-stationary (Eskilson an Claesson 1988)

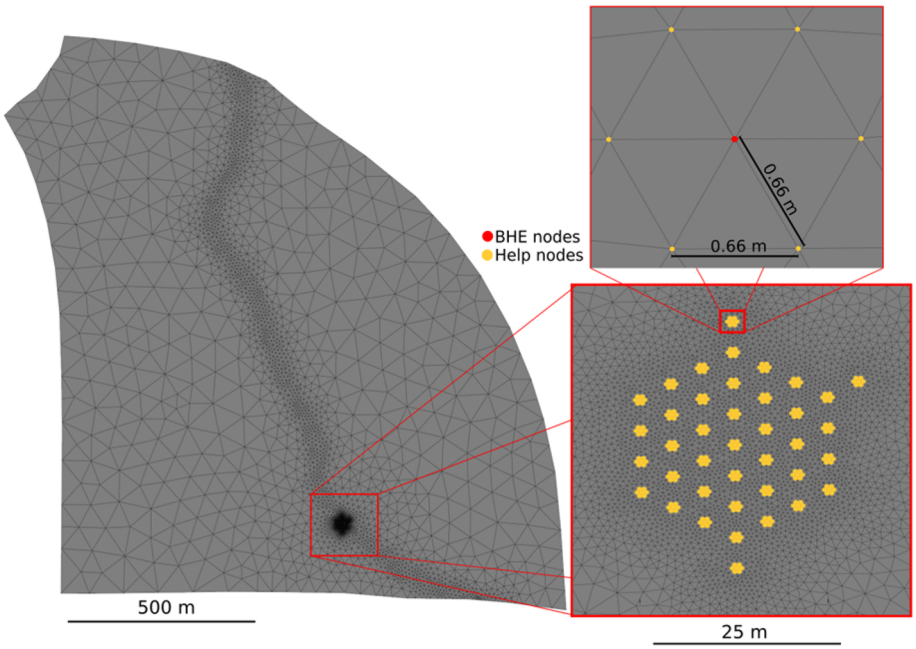

Fig. 6 Model domain with the integrated BHE and the discretization scheme around every BHE node

simulations. It features solving of fluid and heat transport processes in the natural subsurface with a 3D finite element approach. The BHE, in contrast, are computed using an analytical solution (Diersch et al. 2011b; Bauer 2011; Eskilson and Claesson 1988), which is coupled to the finite element mesh along with 1D finite element representations. To ensure an optimal coupling of the BHE solution to the 3D model, the nodes surrounding the BHE (help nodes in Fig. 6) were placed at an optimal node distance (Diersch et al. 2011b; Nillert 1976). The approach was chosen due to its robustness and reasonable accuracy for long-term simulations (Diersch et al. 2011a, b). In a previous study, the simulations agreed with measured data (Mielke et al. 2014).

The geological drilling data were imported from the layer contour map as a point set and interpolated into a meshed surface in FEFLOW. In total, five horizons were imported: the ground surface from a digital elevation model, the base quarternary, the base Rotliegend and the base granodiorite weathering zone. The displacement was assumed to be constant with 30 m for the whole fault. Due to the postulated paleozoic

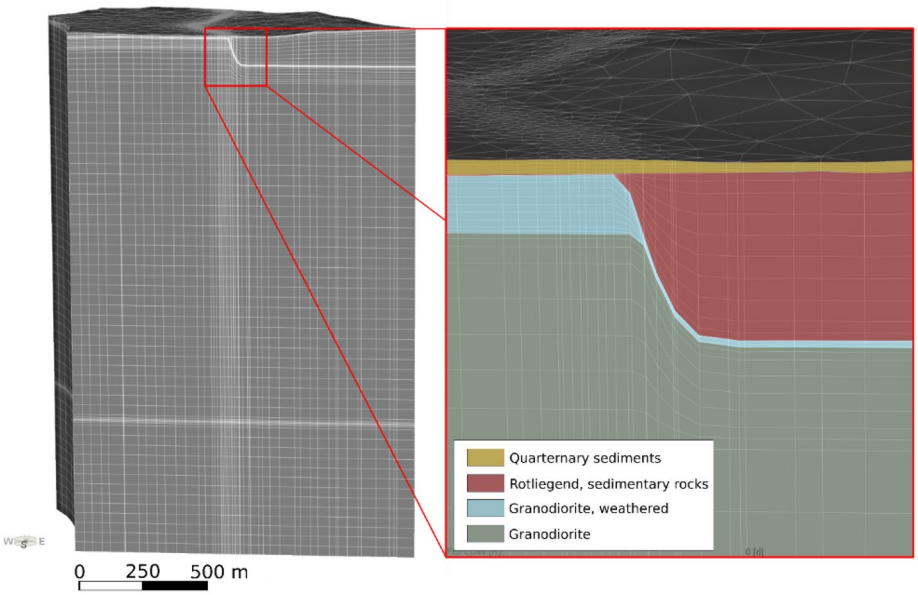

Fig. 7 FEFLOW 3D model with the distribution of the lithologies

Table 2 Assigned thermal and hydraulic properties

Parameter	Quaternary	Rotliegend	Weathered Granodiorite	Granodiorite
Depth (below surface)	0–5 m	5–40 m	5–50 m	50–1000 m
Vol. heat capacity [MJ m^{-3} K^{-1}]	1.45	1.65	1.94	2.12
Thermal conductivity [W m^{-1} K^{-1}]	1.40	2.71	1.13	2.64
Porosity [—]	0.17	0.09	0.17	0.03
Hydraulic conductivity [m s^{-1}]	3.7E—04	6.5E—06	1.15E—04	5.0E—08

weathering of the crystalline, the weathering zone of the granodiorite was continued underneath the Rotliegend, but with reduced thickness (Fig. 7).

This geological model was created using the generated surfaces as a unit basis. One disadvantage of the layered approach is that layers that the fault would cut off still propagate through the whole model domain. The resulting errors were minimized by fitting the respective material properties of the corresponding correct lithology to these elements.

Hydraulic properties

The model is considered to be fully saturated. Three boundary conditions (BC) were assigned. Firstly, hydraulic head BCs (first-order Dirichlet BC) were applied to the northern and southern boundaries. Values for the hydraulic head BC were derived from the groundwater head data as a mean of the values from Fig. 4. Groundwater recharge of 170 mm a^{-1} was assumed for the top of the model, considering an approximate degree of artificial soil sealing of 10% at the Lichtwiese campus (Beier 2008). Hydraulic conductivity parameters (Table 2) for the sedimentary units and the granodiorite weathering zone were extracted from pumping tests at the project site. The hydraulic

conductivity for the basement shown in Table 2 is based on formation permeability data for crystalline rocks (Stober and Bucher 2007).

Thermal properties

For the temperature, two first-order Dirichlet Boundary conditions were applied to the top and bottom of the model. Accordingly, the temperature at 1000 m depth was assumed to be 50 °C (Rühaak et al. 2012), corresponding to a geothermal gradient of 4 °C per 100 m. For the surface temperature, the average temperature in Darmstadt for the years 1981 to 2010 of 10.1 °C was used (DWD 2019). Thermophysical rock properties for the different geologic units (Table 2) were derived from outcrop analog studies of regional outcrops (Bär et al. 2019; Weinert et al. 2020).

Thermal conductivity and volumetric heat capacity are temperature-dependent parameters. The thermal conductivity decreases with increasing temperature, whereas the heat capacity shows the opposite behavior (Mottaghy et al. 2008; Schatz and Simmons 1972; Ahrens 1995). Hence, both parameters were temperature corrected prior to simulation (Vosteen and Schellschmidt 2003; Bär 2012).

Parameter fitting

A parameter fitting for the hydraulic conductivity was conducted, to adjust the hydraulic properties of the model units so that the simulated hydraulic heads fit the field data. The parameter fitting was done with Pest (Doherty 1994) using a pilot point approach (Doherty 2003; Fienen et al. 2009).

Implementation of the permeable fault

With reference to the pre-drill geological and geophysical knowledge, the hydraulic fault properties were initially set to low permeability. While drilling it became obvious that the fault provides a reasonable hydraulic conductivity (e.g., large circulation losses). Therefore, a broader range of fault hydraulic properties was implemented. Exact results for fault permeability can be expected after evaluation of the drilling and pumping data.

The interpreted fault was implemented into the model using a discrete feature element. Discrete feature elements are 1D or 2D objects added to an existing 3D FEFLOW mesh to simulate features with specific flow properties like fractures or faults (DHI WASY 2009). Here, a discrete feature element applying Darcy's law for the fault internal flow simulation was used. As concluded from the evaluated drilling data, the implemented fault zone only interferes with one-half of the borehole storage system (Fig. 8)

Variation of fault parameters

Since the fault zone characteristics are not well known, a parameter variation study was conducted to investigate the effects of different hydraulic conductivities and thicknesses of the fault zone on the temperature field and the storage system performance. Accordingly, the respective properties of the discrete feature elements were varied. In total, 15 models with fault zone thicknesses of 0.5 m, 1 m, 2 m, 3 m, and 4 m and hydraulic conductivities ranging from 10^{-3} m $s^{-1}$and 10^{-4} m s^{-1} to 10^{-5} m s^{-1} were simulated. Fault thicknesses were chosen to get a reasonable contrast between the simulation results.

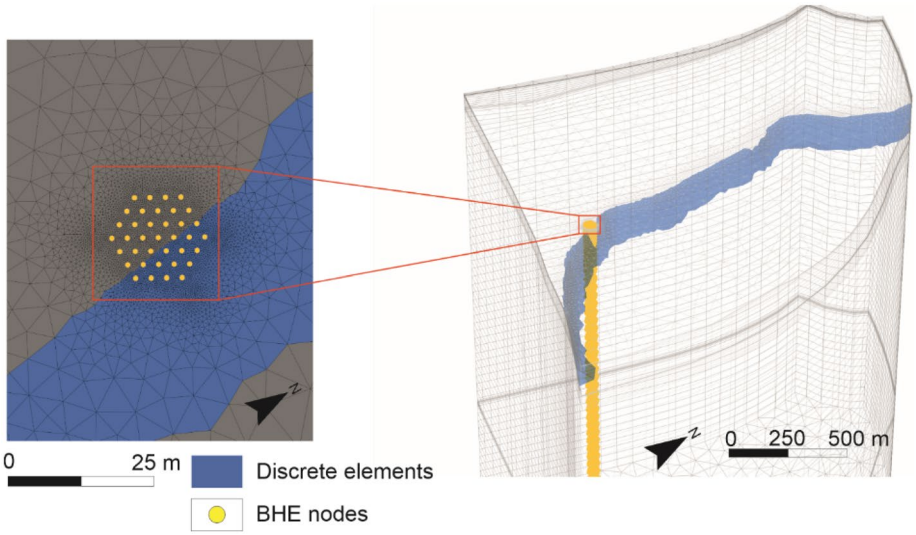

Fig. 8 Position of the fault in the model in the 2D view and 3D view

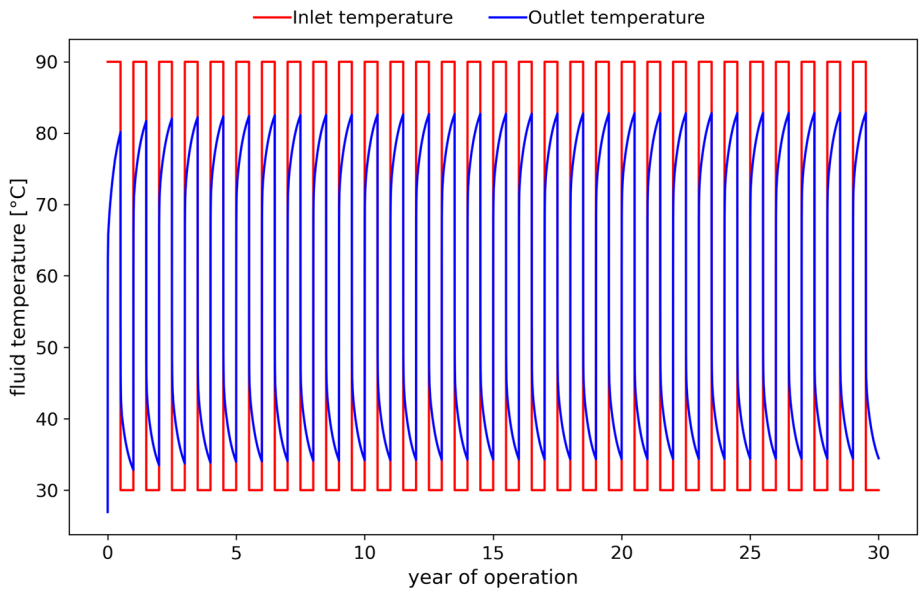

Fig. 9 Exemplary inlet and outlet temperatures for the whole BHE array

Borehole heat exchanger operation scenario

To obtain comparable results, a simplified loading and unloading scheme was applied for every simulation (Fig. 9). During charging periods, the inlet temperature was set to 90 °C. This temperature can be supplied by solar thermal collectors and describes the upper-temperature limit of PE-X pipes (Welsch 2019). During the heat extraction period, the inlet temperature was set to 30 °C to ensure the supply of low-temperature heating systems. Each loading and unloading cycle ran for half a year (183.5 days). The total simulation time is 30 years (10950 days). BHE were connected in parallel to provide a constant inlet temperature for each of them. For the whole simulation time, the flow rate for each BHE was set to 2 l s^{-1}. According to some preliminary

considerations, this value represents a good compromise between a comparably low pressure drop in the BHE and a high heat exchange rate.

Data analysis

Multiple performance indicators were calculated to assess the efficiency of the different models. Firstly, the mean outlet temperature was derived for the whole BHE array as an average of all BHE. Heat is transferred continuously due to the temperature difference between the heat transfer fluid and the surrounding rock. The heat rate $\dot{Q}$, which is the heat exchanged between the heat carrier fluid and the surrounding rock, was calculated with Eq. 1:

$$\dot{Q} = \Delta T \cdot (\rho c)_f \cdot \dot{V}, \tag{1}$$

where ΔT is the difference between inlet and outlet temperature of the heat carrier fluid with a flow rate of $\dot{V}$ through the BHE array. $(\rho c)_f$ is the volumetric heat capacity of the fluid. The fluid parameters were assumed to be constant for the whole temperature range to simplify the system. The total heat stored or extracted could be calculated by integrating exchanged heat over a charging or discharging cycle (1 year). The ratio between the amount of heat stored and extracted is defined in Eq. 2 as the storage efficiency:

$$\mu = \left| \frac{Q_E}{Q_s} \right|, \tag{2}$$

with Q_E being the total amount of heat extracted and Q_s the total amount of heat stored during a period of 1 year.

Results

The sum of stored heat in the different model setups ranges from 456 to 463 GWh over 30 years of operation, constituting only a minor deviation of approximately 1.5%. The amount of heat extracted ranges from 318 to 326 GWh representing a deviation of 2.5%, whereas the storage efficiency ranges from 0.69 to 0.71 depicting a change of 3%. The results for all models are shown in Table 3.

All models investigated display a typical long-term behavior for BTES systems (Welsch et al. 2016). Since a certain amount of heat remains in the reservoir after each extraction and loading cycle, the temperature in the reservoir around the BHE increases throughout the simulation period. Figure 10 reveals that this leads to a decrease in the heat stored and an increase in the heat extracted, which facilitates the rising storage efficiency. This behavior is represented by a sharp increase in storage efficiency in the first years of operation that passes over into a small yearly increase in efficiency for the later simulation stages. The storage efficiency increases in all models from just above 40% to close to 60% in the first year of operation. The heat extracted shows a similar trend with a sharp rise in the first years and a slight but steady increase over the following years. In contrast, the amount of heat stored depicts a substantial decrease for the first years of operation due to the increasing storage temperatures.

Table 3 Simulation results of all models

Hydraulic conductivity [m s^{-1}]	Fault zone thickness [m]				
	0.5	1	2	3	4
	Heat stored [GWh]				
10^{-3}	460.9	462.2	462.8	462.7	462.8
10^{-4}	458.1	458.4	459.1	459.6	458.7
10^{-5}	456.5	456.7	456.7	456.9	457.2
	Heat extracted [GWh]				
10^{-3}	323.5	321.8	321.1	320.9	320.2
10^{-4}	326.2	325.6	324.9	324.2	323.0
10^{-5}	325.5	325.5	325.3	325.3	325.2
	Storage efficiency [-]				
10^{-3}	0.706	0.700	0.698	0.698	0.696
10^{-4}	0.716	0.715	0.712	0.710	0.704
10^{-5}	0.717	0.717	0.717	0.716	0.716

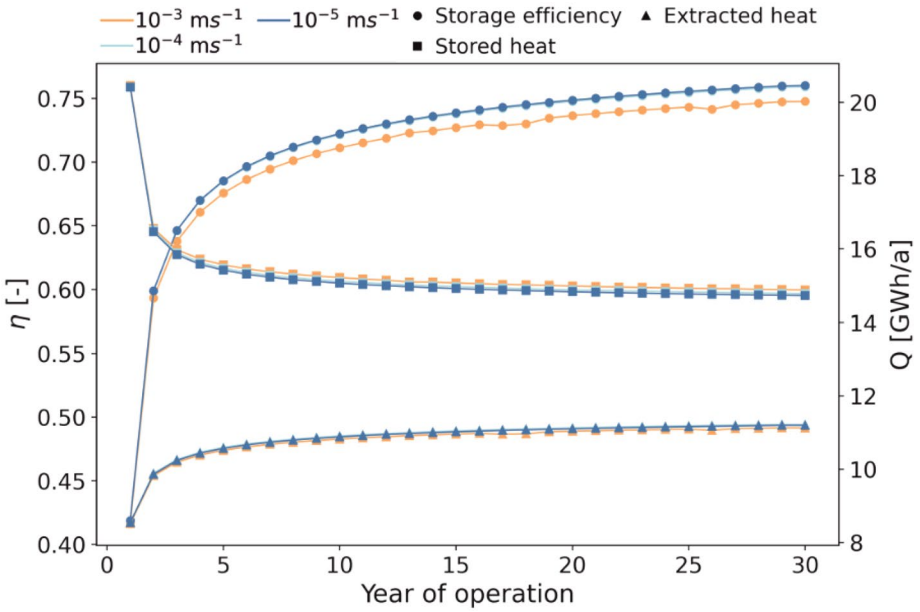

Fig. 10 Storage efficiency, the amount of stored and extracted heat for annual cycles over 30 years of simulation for a fault zone thickness of 0.5 m

Influence of hydraulic conductivity and fault zone thickness

As expected, the amount of stored heat increases with larger hydraulic conductivities of the fault zone for all models (Fig. 11a). The heat extracted is reduced with increasing hydraulic conductivities and fault zone thickness (Fig. 11c). Finally, the storage efficiency is reduced with increased hydraulic conductivities and fault zone thicknesses (Fig. 11e). When analyzing the effect of the fault zone thicknesses on the storage, it becomes apparent that the amount of heat stored increases and the heat extraction decreases with larger fault zone thicknesses (Fig. 11b, d, f). This, in combination, results in higher efficiencies or fault zones with a smaller thickness.

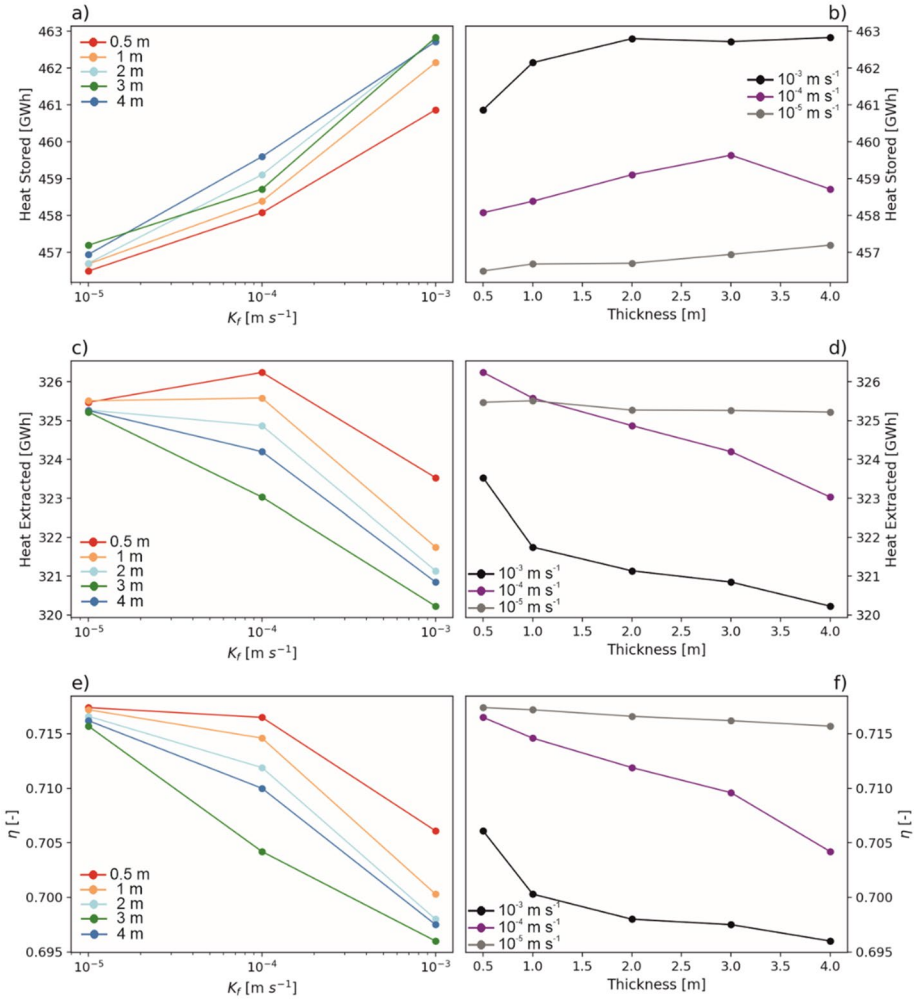

Fig. 11 Influence of the hydraulic conductivity and fault thickness on the amount of heat stored into the MD-BTES, the heat extracted, and the storage efficiency

Influence of the transmissivity

The transmissivity is the product of hydraulic conductivity (K_f) and fault zone thickness (d) (Equation 3):

$$T = K_f \cdot d. \tag{3}$$

The stored heat amounts in the MD-BTES show a steady growth starting at the lowest transmissivities, reaching the highest capacity with 456.5 GWh (Fig. 12d). An opposite behavior is displayed for the heat extracted (Fig. 12e) where the values stay almost constant at first and then diminish for higher hydraulic conductivities. Figure 12f shows the same behavior for storage efficiency.

Variation of the Darcy flux

Table 4 illustrates the variation of Darcy flux for the entire fault surface for the simulated models. A trend with increasing flow velocities for smaller thicknesses and

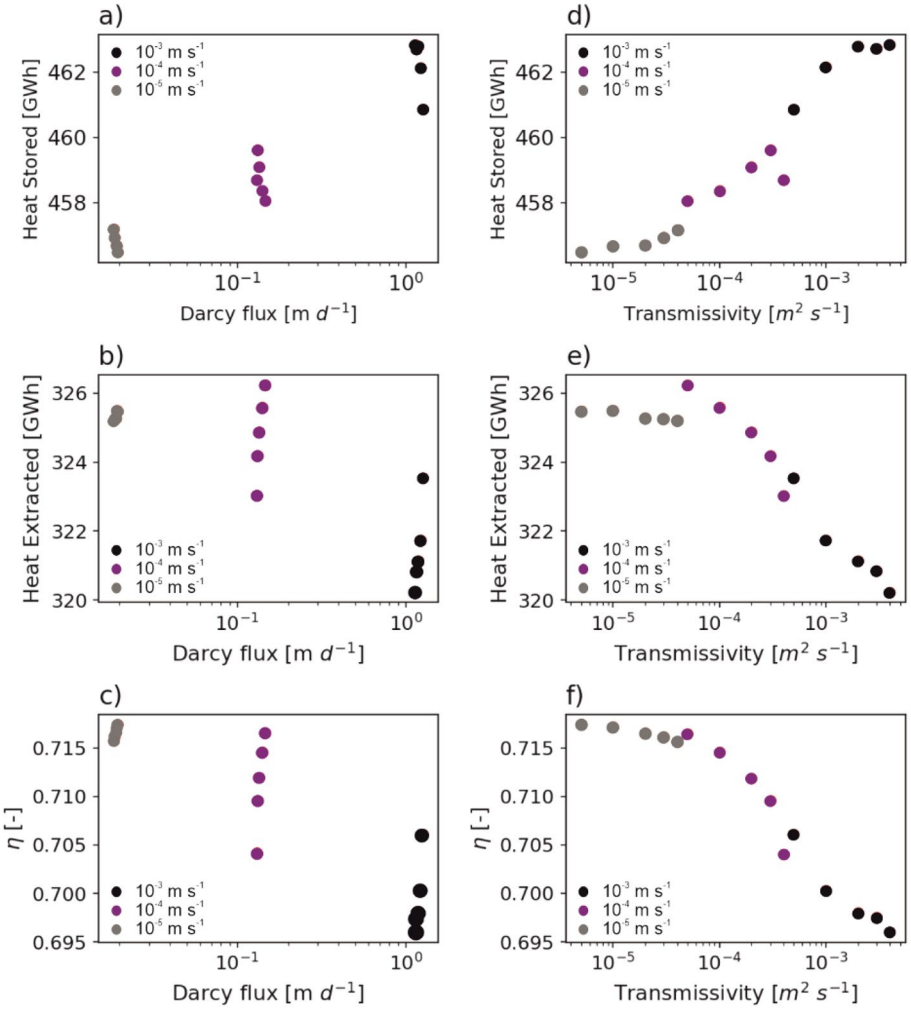

Fig. 12 Influence of the Darcy flux (**a**–**c**) and transmissivity (**d**–**f**) on the amount of heat stored, the heat extracted and the storage efficiency

Table 4 Mean Darcy flux [m d^{-1}] for the whole fault area for the four given hydraulic conductivities

Thickness [m]	Darcy flux [m d^{-1}]		
	[10^{-3} m s^{-1}]	[10^{-4} m s^{-1}]	[10^{-5} m s^{-1}]
0.5	1.26	0.146	0.0194
1	1.23	0.140	0.0193
2	1.19	0.135	0.0190
3	1.16	0.132	0.0187
4	1.14	0.131	0.0185

higher hydraulic conductivities is displayed. This comes to no surprise as the flow cross-section is reduced with reduced thicknesses. A more considerable variability is displayed for heat stored for the models with higher flow velocities. Figure 12 shows

a correlation of larger amounts of heat stored and reduced amounts of heat extracted for increasing Darcy flux. This results in a reduction of storage efficiency.

Heat plume development

The temperature change in the vicinity of the BTES for a constant thickness of 0.5 m and varying hydraulic conductivities is observed for specific models (Fig. 13). As a result of the charging operation, a plume with elevated temperatures develops along the fault zone. As expected, the resulting heat plumes differ with changing hydraulic conductivities of the fault zone. As a measure for the length of the developed heat plume, the transport distance in the fault plane direction of a 1 K temperature increase was chosen. For the models with the highest hydraulic conductivity (10^{-3} m s^{-1}), a temperature increase of 1 K can be traced up to 600 m. For the models with further reduced conductivities of 10^4 m s^1 and 10^5 m $s^{1,}$ the heat plume displays a length of 140 m and 100 m, respectively. The maximum temperature changes observed in the heat plumes decrease with rising hydraulic conductivities. For the lowest hydraulic conductivities, the maximum temperature change mounts to 38 K. With raising conductivity values, it diminishes to 36 K and 26 *K,* respectively.

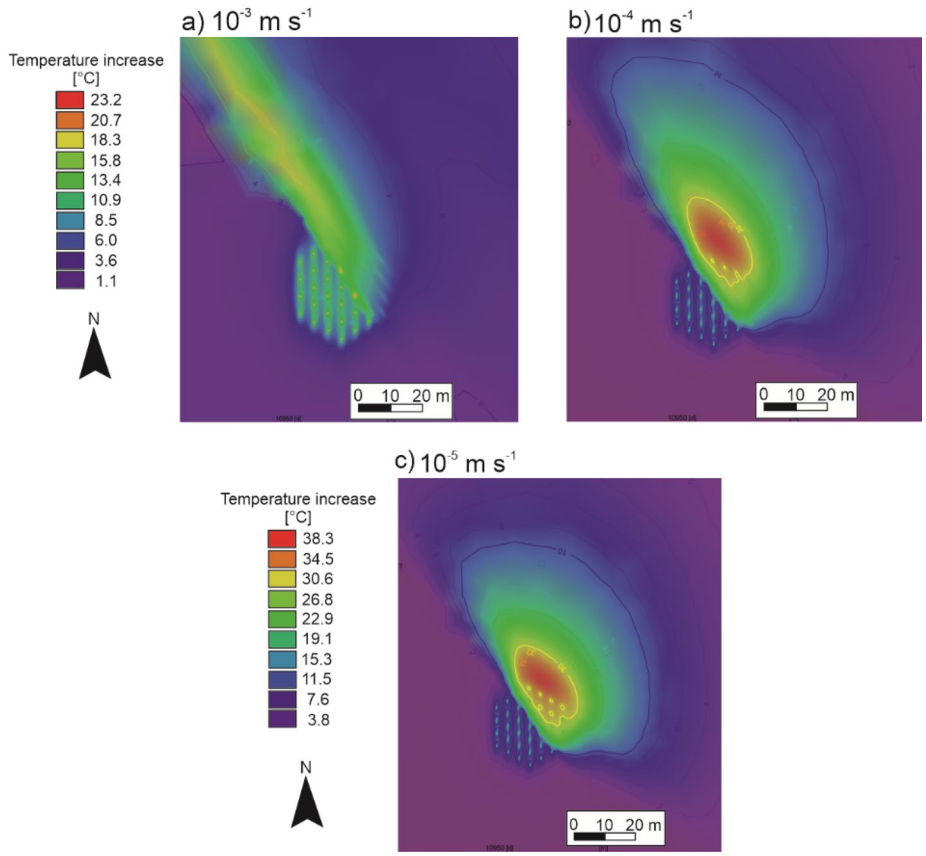

Fig. 13 Resulting heat plumes after a simulation time of 30 years after the last extraction period for a fault with a thickness of 0.5 m and conductivities of **a** 10^3 m s^1, **b** 10^4 m s^1 and **c** 10^5 m s^1

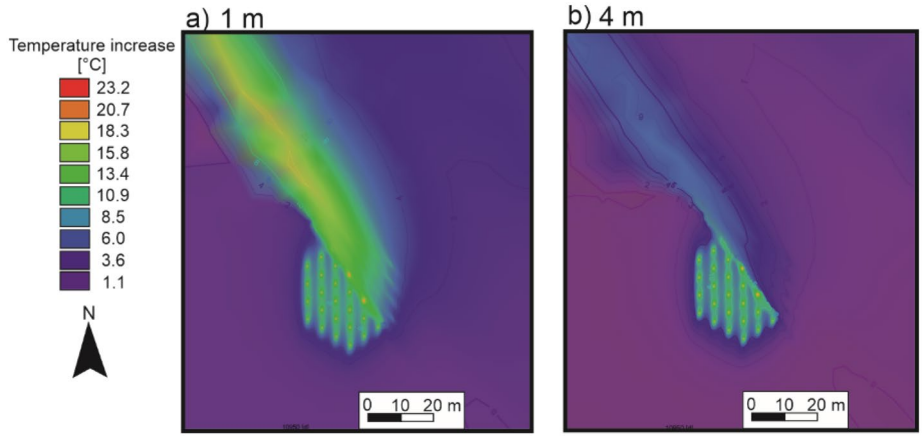

Fig. 14 Heat plumes after a simulation time of 20 years for a constant hydraulic conductivity of 10^3 m s^1 and varying thicknesses of **a** 1 m and **b** 4 m

Furthermore, the heat plume shape changes (Figs. 13 and 14). For the two models with lower conductivity values, the heat diffuses elongated along the fault. In contrast, for the model with the lowest conductivity, the heat is distributed locally over the whole area of the fault. The heat plume size and temperature can be correlated with the measured groundwater flow velocities along the fault plane, leading to more pronounced heat transport from the BTES. Consequently, this lowers the resulting temperatures as well.

When analyzing the heat distribution for the cases with a constant hydraulic conductivity of 10^{-3} m s^{-1} and varying thicknesses, a very similar shape of the heat plume can be observed for every model (Fig. 14). The temperature distribution is changed, but the overall shape of the plume stays constant. With larger fault thicknesses from 0.5 m to 4 m, the maximum temperature change declines from 25 K to 16 K, whereas the heat plume expands from 600 m to 1000 m.

Discussion

Validity of the models

Of course, not all physical details can be represented, and certain simplifications must be accepted. A limiting factor for this study is its simplified approach to fault zone hydrogeology. Following Darcy's law, the fault zone is assumed to be represented by a geometric feature with a defined thickness and hydraulic properties. In reality, fault zones usually consist of a fault core, where most of the displacement is accommodated, and a surrounding damage zone consisting of fractures and secondary faults (Caine et al. 1996; Bense et al. 2013). Depending on the lithology and secondary processes like cementation, fault zones can act as fluid barrier or conduit (Scibek et al. 2016). The damage zone is usually a permeable conduit for crystalline rocks due to enhanced fracture density, while the fault core depicts low permeabilities (Bense et al. 2013; Chester and Logan 1986; Caine et al. 1996). Additionally, the enlarged hydraulic conductivities chosen for this study would represent an extremely permeable fault, which is inadequate in the given geological context, as high clay contents related to the granodiorite weathering were discovered in the evaluated drilling data. Nevertheless,

the impact of such high conductivities was investigated to get a broader picture of the influence of different hydraulic configurations.

Moreover, the discrete feature approach is a strong simplification of fault zone geometry, especially for larger fault thicknesses. Since the discrete feature element cuts the model on one slice only, they might cause an underrepresentation of heat transport as a minimal domain of the model is affected, especially for the larger fault zone thickness models. However, such simulations provide valuable information about the MD-BTES system response to geological heterogeneity.

Another simplification comes along with the very simplified BHE operation scenario. Nevertheless, realistic, fluctuating loading and unloading cycles would add unnecessary noise to the simulation results obscuring the main effects affiliated with the fault zone.

Fault zone influence

The deciding factor is the resulting Darcy flux, which governs the convective heat transport along the fault zone. For higher flow velocities, more of the stored heat gets transported downstream from the storage, resulting in lower efficiencies. Additionally, larger fault thicknesses also induce higher heat losses, which can be attributed to the higher volume flow. Figure 12 illustrates a higher storage efficiency of up to 0.017 for the models with the highest transmissivities. Minima in efficiency and extracted heat of 0.696 and 320.2 GWh and a maximum in heat stored of 462.8 GWh are therefore triggered by high conductivity and large fault zone thickness model with flow velocities of around 1.14 m $days^{-1}$. Figure 12a, b, and c depicts these correlations. The high amounts of heat stored for the models with the lowest efficiency is caused by the increased temperature difference between heat carrier fluid and the subsurface caused by the heat removal through groundwater flow. The heat plume temperature and length are also governed by groundwater flow velocity, which increases heat plume length and reduces heat plume temperature.

During the assessment of the influence of the fault on the MD-BTES, it has to be considered that the implemented fault zone propagates through half of the MD-BTES, and covers a small depth interval given the total depth of the storage system. Considering this, the effect of one highly conductive fault zone on the storage efficiency can be expected to be much higher for smaller storage systems with lower depth-to-width ratios, as a more significant percentage of the storage volume would be affected. Hence, the thermal influence of local fault zones is limited for MD-BTES. Larger zones with enhanced permeabilities in larger fault damage zones are probable to affect the storage efficiency significantly. Additionally, geological heterogeneities potentially impact the directional stability of the drilling process. Since a constant distance between the BHE is critical for the efficiency of the storage (Welsch 2019), all possible causes for directional deviations during the drilling process should be treated very carefully.

Conclusions

This study investigated the effect of a local, permeable fault zone on the energetic performance of a MD-BTES. The results reveal that the impact on the storage is mainly dependent on the hydraulic conductivity of the respective fault zone. The hydraulic conductivity parameter controls the groundwater flow velocity, which ultimately

regulates the fault impact on the storage efficiency. The lowest efficiencies can be observed for fault zones with a high hydraulic conductivity and a large fault zone thickness. In total, a maximum of 462.8 GWh and a minimum of 456.5 GWh were stored in the simulated 30 years of operation. Respectively, a maximum of 326.2 GWh and a minimum of 320.2 GWh could be extracted. This constitutes to a maximal and minimal storage efficiency of 0.717 and 0.696. The small effect of the fault with a maximum deviation of 3% in storage efficiency shows a general advantage of the concept of medium deep borehole heat exchangers. Due to their depth, local zones of increased groundwater flow only have a small impact on the overall system performance. Moreover, areas presenting enhanced fluid flow can be thermally insulated, thereby mitigating their effect on the groundwater. The influence on smaller size borehole heat storage systems can be expected to be more pronounced.

Depending on the loading and unloading scenario of the BTES, permeable zones may significantly increase the heat plume size, which is essential for the groundwater-related approval process by local authorities. In this study increased temperatures of 1 K could be observed up to 1000 m from the storage system.

In the future, further modeling tasks will be conducted in the SKEWS project, following a detailed geophysical campaign to get a better picture of the local geologic context. Following the project realization, the built model will be calibrated with drilling and borehole logging datasets to implement higher precision models with realistic loading and unloading scenarios.

Acknowledgements
We would like to thank the HLNUG for providing digital elevation and drilling data and the TU Darmstadt for granting access to monitoring data of their groundwater monitoring wells.

Author contributions
LSe worked on the data collection and modeling and wrote the manuscript. BWe directed the project, providing ideas and support. MFr helped with the data collection and provided, together with CBo and ISa, useful comments during the writing process. All authors proofread the manuscript, and provided their comments and suggestions. All authors read and approved the final manuscript.

Funding
Open Access funding enabled and organized by Projekt DEAL. The authors acknowledge the financial support by the Federal Ministry for Economic Affairs and Energy of Germany in the project SKEWS (project number 03EE4030A). This research was supported by the Interreg NWE Programme through the Roll-out of Deep Geothermal Energy in North-West Europe (DGE-ROLLOUT) Project (www.nweurope.eu/DGE-ROLLOUT). The Interreg NWE Programme is part of the European Cohesion Policy and is financed by the European Regional Development Funds (ERDF). We acknowledge the support of the Deutsche Forschungsgemeinschaft (DFG – German Research Foundation) and the Open Access Publishing Fund of the Technical University of Darmstadt.

Availability of data and materials
The dataset supporting the conclusions of this article is available in the TU Darmstadt Datalib repository.

Declarations

Competing interests
The authors declare that they have no competing interests.

Received: 12 April 2022 Accepted: 11 August 2022
Published online: 07 September 2022

References

Ahrens TJ, editor. Rock Physics & Phase Relations. Washington: American Geophysical Union; 1995.
Al-Malabeh A, Kempe S. Petrolithology of the Permian melaphyre lavas, Darmstadt. Germany Njgpa. 2009;252(2):129–43. https://doi.org/10.1127/0077-7749/2009/0252-0129.

Aretz A, Bär K, Götz AE, Sass I. Outcrop analogue study of Permocarboniferous geothermal sandstone reservoir formations (northern Upper Rhine Graben, Germany): impact of mineral content, depositional environment and diagenesis on petrophysical properties. Geol Rundsch. 2016;105(5):1431–52. https://doi.org/10.1007/s00531-015-1263-2.
Backhaus E. Die randliche "Rotliegend"-Fazies und die Paläogeographie des Zechsteins im Bereich des nördlichen Odenwalds. Notizblatt Des Hessischen Landesamts Für Bodenforschung. 1965;93:112–40.
Bär K. Untersuchung der tiefengeothermischen Potenziale von Hessen [Dissertation]. Darmstadt: Technische Universität Darmstadt; 2012.
Bär K, Rühaak W, Welsch B, Schulte D, Homuth S, Sass I. Seasonal High Temperature Heat Storage with Medium Deep Borehole Heat Exchangers. Energy Procedia. 2015;76:351–60. https://doi.org/10.1016/j.egypro.2015.07.841.
Bauer D. Zur thermischen Modellierung von Erdwärmesonden und Erdsonden-Wärmespeichern [Dissertation]. Stuttgart: Universität Stuttgart; 2011.
Beier M. Urbane Beeinflussung des Grundwassers: Urbane Beeinflussung des Gundwassers: Stoffemissionen und -immissionen am Beispiel Darmstadts [Dissertation]. Darmstadt: Technische Universität Darmstadt; 2008.
Bense VF, Gleeson T, Loveless SE, Bour O, Scibek J. Fault zone hydrogeology. Earth Sci Rev. 2013;127:171–92. https://doi.org/10.1016/j.earscirev.2013.09.008.
Blöcher G, Reinsch T, Regenspurg S, Henninges J, Brehme M, Saadat A, et al. Geothermie in Urbanen Räumen : Thermische Untergrundspeicherung Und Tiefe Geothermie in Deutschland. 2019. https://doi.org/10.2312/GFZ.syserde.09.01.1.
BMWI. Endenergieverbrauch nach Anwendungsbereichen. 2020.
Caine JS, Evans JP, Forster CB. Fault zone architecture and permeability structure. Geol. 1996;24(11):1025. https://doi.org/10.1130/0091-7613(1996)024%3c1025:FZAAPS%3e2.3.CO;2.
Chen C, Shao H, Naumov D, Kong Y, Tu K, Kolditz O. Numerical investigation on the performance, sustainability, and efficiency of the deep borehole heat exchanger system for building heating. Geotherm Energy. 2019. https://doi.org/10.1186/s40517-019-0133-8.
Chester FM, Logan JM. Implications for mechanical properties of brittle faults from observations of the Punchbowl fault zone. California PAGEOPH. 1986;124(1–2):79–106. https://doi.org/10.1007/BF00875720.
Derer CE, Schumacher ME, Schäfer A. The northern Upper Rhine Graben: basin geometry and early syn-rift tectono-sedimentary evolution. Int J Earth Sci (geol Rundsch). 2005;94(4):640–56. https://doi.org/10.1007/s00531-005-0515-y.
Diersch HJG. FEFLOW: Finite Element Modeling of Flow, Mass and Heat Transport in Porous and Fractured Media. Berlin: Springer; 2014.
Diersch H-J, Bauer D, Heidemann W, Rühaak W, Schätzl P. Finite element modeling of borehole heat exchanger systems. Comput Geosci. 2011a;37(8):1122–35. https://doi.org/10.1016/j.cageo.2010.08.003.
Diersch H-J, Bauer D, Heidemann W, Rühaak W, Schätzl P. Finite element modeling of borehole heat exchanger systems. Comput Geosci. 2011b;37(8):1136–47. https://doi.org/10.1016/j.cageo.2010.08.002.
Dincer I, Rosen MA. A Unique Borehole Thermal Storage System at University of Ontario Institute of Technology. In: Paksoy HÖ, editor. Thermal Energy Storage for Sustainable Energy Consumption. Dordrecht: Springer, Netherlands; 2007. p. 221–8.
Doherty J. PEST: A Unique Computer Program for Model-independent Parameter Optimisation. International Association of Hydrogeologists. Congress. 1994:551–4.
Doherty J. Ground water model calibration using pilot points and regularization. Groundwater. 2003;41(2):170–7. https://doi.org/10.1111/j.1745-6584.2003.tb02580.x.
Dörr W, Stein E. Precambrian basement in the Rheic suture zone of the Central European Variscides (Odenwald). Int J Earth Sci (geol Rundsch). 2019;108(6):1937–57. https://doi.org/10.1007/s00531-019-01741-7.
DWD. Temperatur: vieljährige Mittelwerte 1981 - 2010. 2019. https://www.dwd.de/DE/leistungen/klimadatendeutschland/mittelwerte/temp_8110_akt_html.html?view=nasPublication&nn=16102. Accessed 24 Jun 2020.
Eskilson P, Claesson J. Simulation model for thermally interacting heat extraction boreholes. Numerical Heat Transfer. 1988;13(2):149–65. https://doi.org/10.1080/10407788808913609.
Fahlbusch K. Störungszonen an den Rheingraben-Schultern (Hardt, Darmstadt) mit Hinweisen auf junge Bewegungen. Notizblatt Des Hessischen Landesamts Für Bodenforschung. 1975;103:315–26.
Fahlbusch K. Die geologischen Grundlagen der alten Wasserversorgung Darmstadts. Notizblatt Des Hessischen Landesamts Für Bodenforschung. 1980;108:223–40.
Fienen MN, Muffels CT, Hunt RJ. On constraining pilot point calibration with regularization in PEST. Groundwater. 2009;47(6):835–44. https://doi.org/10.1111/j.1745-6584.2009.00579.x.
Gehlin S. Borehole thermal energy storage. In: Rees SJ, editor. Advances in ground-source heat pump systems. Duxford: Woodhead Publishing is an imprint of Elsevier; 2016. p. 295–327.
Greifenhagen G. Untersuchungen zur Hydrogeologie des Stadtgebietes Darmstadt mit Hilfe eines Grundwasserinformationssystems unter Verwendung von einer Datenbank, Datenmodellierung und ausgewählten statistischen Methoden [Dissertation]. Darmstadt: Technische Universität Darmstadt; 2000.
Griebler C, Kellermann C, Stumpp C, Hegle F. Auswirkungen thermischer Veränderungen infolge der Nutzung oberflächennaher Geothermie auf die Beschaffenheit des Grundwassers und seiner Lebensgemeinschaften – Empfehlungen für eine umweltverträgliche Nutzung. Umweltbundesamt. 2015.
HLNUG. Geologische Übersichtskarte von Hessen 1:300000. Wiesbaden: Hessisches Landesamt für Naturschutz, Umwelt und Geologie; 2007.
HLNUG. Hessische Bohrdatenbank. Wiesbaden: Hessisches Landesamt für Naturschutz, Umwelt und Geologie; 2020.
Kempe S, Strassenburg J, Belzer S, Henschel H-V, Fahlbusch K. Der Darmstädter Granodiorit im Stollen in der der Dieburger Straße, Mathildenhöhe, Darmstadt. Jahresberichte Und Mitteilungen Des Oberrheinischen Geologischen Vereins. 2001;17:51–63.
Klemm G. Geologische Karte von Hessen 1:25000, Blatt 6118 Darmstadt Ost, 4. Auflage; 1911.
Klemm G. Erläuterungen zur Geologischen Karte Blatt 6118 Darmstadt-Ost (ehem. Blatt Roßdorf). 3rd ed.; 1938.
Kohl T, Brenni R, Eugster W. System performance of a deep borehole heat exchanger. Geothermics. 2002;31(6):687–708. https://doi.org/10.1016/S0375-6505(02)00031-7.

Kranz S, Frick S. Efficient cooling energy supply with aquifer thermal energy storages. Appl Energy. 2013;109:321–7. https://doi.org/10.1016/j.apenergy.2012.12.002.
Lang S, Hornung J, Krbetschek M, Ruckwied K, Hoppe A. Tektonik und Sedimentation am Rand des Oberrheingrabens in Darmstadt im Mittel- und Oberpleistozän. Geologisches Jahrbuch Hessen. 2011;137:19–53.
Liu J, Wang F, Cai W, Wang Z, Li C. Numerical investigation on the effects of geological parameters and layered subsurface on the thermal performance of medium-deep borehole heat exchanger. Renewable Energy. 2020;149:384–99. https://doi.org/10.1016/j.renene.2019.11.158.
Luo Y, Xu G, Cheng N. Proposing stratified segmented finite line source (SS-FLS) method for dynamic simulation of medium-deep coaxial borehole heat exchanger in multiple ground layers. Renewable Energy. 2021;179:604–24. https://doi.org/10.1016/j.renene.2021.07.086.
Mezger JE, Felder M, Harms F-J. Crystalline rocks in the maar deposits of Messel: key to understand the geometries of the Messel Fault Zone and diatreme and the post-eruptional development of the basin fill. zdgg. 2013;164(4):639–62. https://doi.org/10.1127/1860-1804/2013/0034.
Mielke P, Bauer D, Homuth S, Götz AE, Sass I. Thermal effect of a borehole thermal energy store on the subsurface. Geotherm Energy. 2014. https://doi.org/10.1186/s40517-014-0005-1.
Mottaghy D, Vosteen H-D, Schellschmidt R. Temperature dependence of the relationship of thermal diffusivity versus thermal conductivity for crystalline rocks. Int J Earth Sci (geol Rundsch). 2008;97(2):435–42. https://doi.org/10.1007/s00531-007-0238-3.
Nillert P. Beitrag zur Simulation von Brunnen als innere Randbedingungen in horizontalebenen diskreten Grundwasserstromungsmodellen (simulation of wells as inner boundary conditions for horizontal 2D discrete groundwater flow models) [Dissertation]. Dresden: Technische Universität Dresden; 1976.
Reuss M. The use of borehole thermal energy storage (BTES) systems. In: Advances in Thermal Energy Storage Systems. New York: Elsevier; 2015. p. 117–147.
Rühaak W, Bär K, Sass I. Estimating the subsurface temperature of Hessen/Germany based on a GOCAD 3D structural model-a comparison of numerical and geostatistical approaches. EGU 2012.
Sass I, Welsch B, Schulte D. Mitteltiefe Erdwärmesondenspeicher – Lösung für den Nutzungskonflikt Grundwasserschutz versus Geothermienutzung? Bochumer Geowissenschaftliche Arbeiten. 2016;(23):9–17.
Schatz JF, Simmons G. Thermal conductivity of Earth materials at high temperatures. J Geophys Res. 1972;77(35):6966–83. https://doi.org/10.1029/JB077i035p06966.
Schaumann G, Schmitz KW. Kraft-Wärme-Kopplung. 4th ed. Berlin: Springer; 2010.
Schulte DO, Rühaak W, Oladyshkin S, Welsch B, Sass I. Optimization of medium-deep borehole thermal energy storage systems. Energy Technol. 2016a;1(4):104–13. https://doi.org/10.1002/ente.201500254.
Schulte DO, Welsch B, Boockmeyer A, Rühaak W, Bär K, Bauer S, Sass I. Modeling insulated borehole heat exchangers. Environ Earth Sci. 2016b. https://doi.org/10.1007/s12665-016-5638-x.
Schulte DO, Rühaak W, Welsch B, Sass I. BASIMO – Borehole Heat Exchanger Array Simulation and Optimization Tool. Energy Procedia. 2016c;97:210–7. https://doi.org/10.1016/j.egypro.2016.10.057.
Schumacher ME. Upper Rhine Graben: Role of preexisting structures during rift evolution. Tectonics. 2002;21(1):6–17. https://doi.org/10.1029/2001TC900022.
Scibek J, Gleeson T, McKenzie JM. The biases and trends in fault zone hydrogeology conceptual models: global compilation and categorical data analysis. Geofluids. 2016;16(4):782–98. https://doi.org/10.1111/gfl.12188.
Stein E. The geology of the Odenwald Crystalline Complex. Mineral Petrol. 2001;72:7–28. https://doi.org/10.1007/s007100170024.
Stober I, Bucher K. Hydraulic properties of the crystalline basement. Hydrogeol J. 2007;15(2):213–24. https://doi.org/10.1007/s10040-006-0094-4.
Vosteen H-D, Schellschmidt R. Influence of temperature on thermal conductivity, thermal capacity and thermal diffusivity for different types of rock. Phys Chem Earth. 2003;28(9–11):499–509. https://doi.org/10.1016/S1474-7065(03)00069-X .
Weinert S, Bär K, Sass I. Petrophysical Properties of the Mid-German Crystalline High: A Database 1 for Bavarian, Hessian, Rhineland-Palatinate and Thuringian Outcrops. Institut für Angewandte Geowissenschaften, Darmstadt; 2020.
Welsch B. Technical, Environmental and Economic Assessment of Medium Deep Borehole Thermal Energy Storage Systems [Dissertation]. Darmstadt: Technische Universität Darmstadt; 2019.
Welsch B, Rühaak W, Schulte DO, Bär K, Sass I. Characteristics of medium deep borehole thermal energy storage. Int J Energy Res. 2016;13(40):1855–68. https://doi.org/10.1002/er.3570.
Welsch B, Göllner-Völker L, Schulte DO, Bär K, Sass I, Schebek L. Environmental and economic assessment of borehole thermal energy storage in district heating systems. Appl Energy. 2018;216:73–90. https://doi.org/10.1016/j.apenergy.2018.02.011.

Publisher's Note